MOLECULAR
METABOLISM

Proteasome dysfunction disrupts adipogenesis and induces inflammation via ATF3

Check for updates

Nienke Willemsen [1], Isabel Arigoni [1], Maja Studencka-Turski [2], Elke Krüger [2], Alexander Bartelt [1,3,4,5,*]

ABSTRACT

Objective: Regulation of proteasomal activity is an essential component of cellular proteostasis and function. This is evident in patients with mutations in proteasome subunits and associated regulators, who suffer from proteasome-associated autoinflammatory syndromes (PRAAS). These patients display lipodystrophy and fevers, which may be partly related to adipocyte malfunction and abnormal thermogenesis in adipose tissue. However, the cell−intrinsic pathways that could underlie these symptoms are unclear. Here, we investigate the impact of two proteasome subunits implicated in PRAAS, Psmb4 and Psmb8, on differentiation, function and proteostasis of brown adipocytes.
Methods: In immortalized mouse brown pre-adipocytes, levels of *Psmb4*, *Psmb8*, and downstream effectors genes were downregulated through reverse transfection with siRNA. Adipocytes were differentiated and analyzed with various assays of adipogenesis, lipogenesis, lipolysis, inflammation, and respiration.
Results: Loss of Psmb4, but not Psmb8, disrupted proteostasis and adipogenesis. Proteasome function was reduced upon Psmb4 loss, but partly recovered by the activation of Nuclear factor, erythroid-2, like-1 (Nfe2l1). In addition, cells displayed higher levels of surrogate inflammation and stress markers, including Activating transcription factor-3 (Atf3). Simultaneous silencing of *Psmb4* and *Atf3* lowered inflammation and restored adipogenesis.
Conclusions: Our study shows that Psmb4 is required for adipocyte development and function in cultured adipocytes. These results imply that in humans with *PSMB4* mutations, PRAAS-associated lipodystrophy is partly caused by disturbed adipogenesis. While we uncover a role for Nfe2l1 in the maintenance of proteostasis under these conditions, Atf3 is a key effector of inflammation and blocking adipogenesis. In conclusion, our work highlights how proteasome dysfunction is sensed and mitigated by the integrated stress response in adipocytes with potential relevance for PRAAS patients and beyond.

1. INTRODUCTION

Maintenance and regulation of the proteome by the ubiquitin-proteasome system (UPS) is essential for cellular function and health. Degradation of unwanted, obsolete, or damaged proteins by UPS is critical for cells to respond to environmental cues such as nutrients, temperature, or other forms of stress. Failure of the UPS is associated with severe consequences for cellular and systemic health. Case in point, humans with mutations in genes coding for proteasomal subunits or their associated regulators, suffer from immuno-metabolic disorders. These diseases are characterized by a spectrum of rare auto-inflammatory syndromes known as proteasome associated auto-inflammatory syndromes (PRAAS), Chronic Atypical Neutrophilic Dermatosis with Lipodystrophy and Elevated Temperature (CANDLE) [1], Nakajo-Nishimura syndrome, or Joint Contractures-Muscular

atrophy-microcytic anemia-Panniculitis-associated lipodystrophy (JMP) syndrome [2−4]. The first discovered cause of PRAAS was a missense mutation in the gene coding for proteasome subunit beta 8 (*PSMB8,* also known as *LMP7*) [1], and since then, other loss-of-function mutations have been revealed as underlying causes, including proteasome subunit beta 4 (*PSMB4*) [5]. The disease symptoms in patients, which include sterile inflammation by increased production of type I interferons (IFNs) and lipodystrophy, are likely a complex result of disturbed UPS and maladaptive activation of the unfolded protein response (UPR) [6].
The PRAAS-related genes *PSMB4* and *PSMB8* are coding for subunits of the proteasome, a complex that degrades obsolete or damaged proteins to peptides. PSMB4 and PSMB8 are subunits in the 20S core particle of the proteasome, which is a barrel-shaped structure of four heptameric rings of in total 28 subunits with a conserved modular

1

Brief Communication

architecture of $\alpha_{1-7}\beta_{1-7}\beta_{1-7}\alpha_{1-7}$. The active catalytic sites β1, β2, and β5 are located within this structure, which conceals them from the cytosol. The 20S core proteasome is associated with 19S regulator complexes to recognize, bind, and unfold ubiquitin-modified substrates for degradation. This allows for selective degradation of substrates that are translocated into the barrel [7]. The modular structure of the proteasome is also evident in the diversity of isoforms with either alternative active sites or regulator complexes. The constitutive 26S proteasome is ubiquitously found in most cell types and is responsible for the bulk of protein degradation, as well as controls many cellular pathways including signaling, metabolism, and proliferation [8]. Immunoproteasomes bear alternative active sites, and are permanently expressed in cells of hematopoietic origin, but can be induced in response to interferons in other cell types [9]. Immunoproteasomes are implicated in MHC-class I antigen processing, but also in many processes beyond the immune response, such as cell differentiation [9]. Whereas PSMB4/β7, is a subunit of all proteasome isoforms, PSMB8/β5i, is an inducible subunit that replaces β5 in the constitutive proteasome when the proteasome is being remodeled to an immunoproteasome [10].

PRAAS patients display several pathologies with varying degrees of severity, and aberrant inflammation and metabolic dysfunction are major hallmarks of the disease. Among these, the lipodystrophy phenotype is currently not well understood. Classically, lipodystrophy is caused by dysfunction of adipocytes, especially the ability to form healthy fat cells [11], but if PRAAS mutations cause cell-intrinsic differentiation defects or dysfunction of adipocytes has not been explored, yet. In addition, PRAAS patients suffer from recurrent fever flares, which are thought to be caused by inflammation in the central nervous system. However, body temperature is a result of several mechanisms, including adaptive thermogenesis, and it is possible that aberrant thermogenesis is involved in the pathology of PRAAS.

Brown adipose tissue (BAT) is a highly adaptive mammalian organ that is responsible for non-shivering thermogenesis (NST) [12]. Stimulated by cold-induced norepinephrine (NE) and other stimuli, brown adipocytes generate heat through activity of uncoupling protein-1 (Ucp1) and other thermogenic mechanisms. The herewith associated oxidative respiration is highly energy demanding, and is fueled by intracellular and circulating nutrients [13]. Prolonged cold exposure leads to remodeling of BAT [12], which induces proteotoxic pressure on brown adipocytes [14]. We have previously shown that an adaptive increase in proteasomal activity was essential for the maintenance of NST [15]. Adapting proteasomal activity to meet proteolytic demands is mediated by the transcription factor Nuclear factor erythroid-2, like-1 (Nfe2l1, also known as Nrf1 or TCF11). In most cell types, Nfe2l1 is continuously degraded by the proteasome, but it escapes its degradation when proteotoxic stress is increased in the cell, e.g., in the presence of chemical proteasome inhibitors. In that case, Nfe2l1 is cleaved from the ER membrane by the aspartyl protease DNA Damage Inducible 1 Homolog 2 (DDI2), translocates to the nucleus, and initiates the transcription of proteasome subunits, which results in restoration or heightening of proteasomal capacity [16,17]. Lack of Nfe2l1 is associated with diminished NST, marked adipose tissue inflammation, and insulin resistance [15]. Nfe2l1 was previously suggested to play a role in the disease mechanisms of PRAAS [6], but to the best of our knowledge no experimental evidence exists that Nfe2l1 is involved. Based on these findings, we hypothesized that compromised proteasome function, initiated by loss of PRAAS-related Psmb4 or Psmb8, impacts brown adipocyte proteostasis, development, function, and inflammation.

2. MATERIALS AND METHODS

2.1. Mice husbandry and tissue collection

All animal experiments were performed with approval of the local authorities (License: ROB-55.2-2532.Vet_02-30-32). Psmb8 whole-body knock-out mice were described previously [18,19]. Animals were housed in individually ventilated cages at room temperature (22 °C), with a 12-h light−dark cycle, and fed chow-diet (Sniff) and water ad libitum. For cold exposure, wild-type C57BL/6J mice (Janvier) were housed at 30 °C or 4 °C for seven days. Mice were killed by cervical dislocation. Tissues were snap-frozen in liquid nitrogen and stored at −80 °C.

2.2. Cell culture, treatments, and reverse transfection

For cellular experiments, we used immortalized WT-1 mouse brown preadipocytes and 3T3-L1 mouse white preadipocytes. The cells were grown in DMEM Glutamax (Thermo Fisher, supplemented with 10% v/v FBS (Sigma) and 1% v/v PenStrep (Thermo), and incubated 37 °C, 5% CO_2. They were continuously kept between 20 and 80% confluency and split two or three times per week. Cells were used until their passage number exceeded 18. For differentiation, cells were grown to 90−100% confluency. Then, WT-1 cells were differentiated in WT-1 induction medium (850 nM insulin (Sigma), 1 μM dexamethasone (Sigma), 1 μM T3 (Sigma), 1 μM rosiglitazone (Cayman), 500 nM IBMX (Sigma) and 125 nM indomethacin (Sigma)) from day 0 to day 2, and in WT-1 differentiation medium (1 μM T3 and 1 μM rosiglitazone) from day 2 up until day 5, with the medium being replaced every other day. 3T3-L1 cells were differentiated in 3T3-L1 differentiation medium (850 nM insulin (Sigma), 1 μM dexamethasone (Sigma), 1 μM rosiglitazone, and 500 nM IBMX) from day 0 up until day 5, with the medium replaced every other day. For in vitro treatments, differentiated cells were treated with DMSO, 100 nM Epoxomicin (Millipore) or 100 nM Bortezomib (Selleck) for 6 h, 100 nM ONX0914 (Adooq) for 6 h, 1 μM NE (Sigma) for 1 h, or 1 μM CL316,143 (Tocris) for 16 h. For in vitro gene silencing, mRNA levels of target genes were knocked down through reverse transfection with SMARTpool silencing RNA (siRNA, Dharmacon) in Lipofectamine RNAiMAX transfection reagent (Thermo Fisher), used according to manufacturer's instructions. siRNAs were added to the cells in 30 nM for single knock-down or two times 30 nM for double knockdown. Reverse transfection took place 1 day before induction. The transfection mix was replaced for standard induction medium 24 h after transfection. Cells were harvested as preadipocytes, early adipocytes, or mature adipocytes; on day 0, day 3 or day 5 of differentiation, respectively. If not further specified, assays were performed on mature adipocytes, i.e., day 5.

2.3. Gene expression analysis

We used NucleoSpin RNA kit (Macherey Nagel), according to the manufacturer's instructions, for RNA extraction. RNA concentrations were then measured with a NanoDrop spectrophotometer (Thermo Fisher). Complementary DNA (cDNA) was prepared by adding 2 μl Maxima H Master Mix (Thermo Fisher) to 500 ng RNA, adjusted with H_2O to 10 μl total. This cDNA mixture was diluted 1:40 in H_2O. Relative gene expression was measured with qPCR. Per reaction, 4 μL cDNA, 5 μL PowerUp™ SYBR Green Master Mix (Applied Biosystems) and 1 μL of 5 μM primer stock (Sigma, see Supplementary Table 1 for sequences) were mixed. Expression was measured in a Quant-Studio 5 RealTime PCR system (Thermo Fisher, 2 min 50 °C, 10 min 95 °C, 40 cycles of 15 s 95 °C, 1 min 60 °C). Cycle thresholds (Cts) of genes of interest were normalized to TATA-box binding protein (Tbp) levels by the ΔΔCt-method. Relative gene expression is displayed as relative

copies per *Tbp* or as fold change to the appropriate experimental control groups.

2.4. Protein isolation and analysis

The samples were lysed in RIPA buffer (50 mM Tris (Merck, pH = 8), 150 mM NaCl (Merck), 5 mM EDTA (Merck), 0.1% w/v SDS (Carl Roth), 1% w/v IGEPAL® CA-630 (Sigma–Aldrich), 0.5% w/v sodium deoxycholate (Sigma–Aldrich)) freshly supplemented with protease inhibitors (Sigma–Aldrich) in a 1:100 ratio. Cell lysates were centrifuged for 30 min (4 °C, 21,000 *g*) and tissue lysates were centrifuged 3 times 30 min, before supernatant was collected. Protein concentrations were determined using the Pierce BCA assay (Thermo Fisher) according to the manufacturer's instructions. 15–30 μg protein per sample were denatured with 5% vol/vol 2-mercaptoethanol (Sigma) for 5 min at 95 °C before they were loaded in Bolt™ 4–12% Bis-Tris gels (Thermo Fisher). After separation, proteins were transferred onto a 0.2 μm PVDF membrane (Bio-Rad) using the Trans-Blot® Turbo™ system (Bio-Rad) at 12 V, 1.4 A for 16 min. The membrane was briefly stained with Ponceau S (Sigma) to verify protein transfer and consequently blocked in Roti-Block (Roth) for 1 h at room temperature. The membranes were incubated overnight in primary antibody dilutions (1:1000 in Roti-block) at 4 °C. The following primary antibodies were used: β-tubulin (Cell Signaling, 2146), Psmb4 (Santa Cruz, sc-390,878), Psmb8 (Cell Signaling, 13,635), Nfe2l1 (Cell Signaling, 8052), Ubiquitin/P4D1 (Cell Signaling, 3936), Ucp1 (Abcam, ab10983), and Proteasome 20S alpha 1 + 2+3 + 5+6 + 7 (Abcam, ab22674). After washing with TBS-T (200 mM Tris (Merck), 1.36 mM NaCl (Merck), 0.1% v/v Tween 20 (Sigma)), the membranes were incubated in secondary antibody (Santa Cruz) solutions (1:10,000 in Roti-block) for 90 min at room temperature. The membranes were washed in TBS-T and developed using SuperSignal West Pico PLUS Chemiluminescent Substrate (Thermo Fisher) in a Chemidoc imager (Bio-Rad). The uncropped blot images can be found in the Supplementary Fig. S1.

2.5. Oil Red O staining

We used Oil Red O (ORO) staining to measure lipid content in adipocytes. Cells were washed with cold DPBS (Gibco), fixed in zinc formalin solution (Merck) for 60 min at room temperature, and then again washed the cells with DPBS. After the samples had completely dried, they were stained with ORO mix (60% v/v Oil-Red-O solution (Sigma), 40% v/v H$_2$O) for 60 min. After the incubation time, the cells were washed several times with water. We took pictures to visualize lipid content. To quantify lipid content, the ORO staining was eluted with 100% isopropanol, and the absorption was measured at 500 nm in a Tecan plate reader.

2.6. Free glycerol assay

To assess lipolysis, we used Free Glycerol Reagent (Sigma F6428) and Glycerol standard solution (Sigma G7793) to measure free glycerol concentrations in the cell culture supernatant. After treatment and just before harvesting the samples, we collected cell culture medium to measure free glycerol content. The kit was used according to manufacturer's instructions. For normalization, we measured protein content with Pierce BCA assay.

2.7. Proteasome activity

To prepare lysates for the proteasomal activity assay, cells were lysed in lysis buffer (40 mM TRIS pH 7.2 (Merck), 50 nM NaCl (Merck), 5 mM MgCl$_2$(6H$_2$O) (Merck), 10% v/v glycerol (Sigma), 2 mM ATP (Sigma), 2 mM 2-mercaptoethanol (Sigma). Activity was measured using the Proteasome Activity Fluorometric Assay II kit (UBPBio, J41110), according to manufacturer's instructions in a Tecan Plate reader. This

assay allowed for measurements of chymotrypsin-like, trypsin-like, and caspase-like activity. The results were then normalized to either protein, using Bio-Rad Protein Assay Kit II (Bio-Rad), or DNA, using the Quant-iT PicoGreen dsDNA assay kit (Invitrogen, P7589), both according to manufacturer's instructions.

2.8. Native PAGE

The protocol for in-gel proteasome activity assay and subsequent immunoblotting was previously described in detail [20]. In short, cells were lysed in Lysis buffer (50 mM Tris/HCl pH 7.5, 2 mM DTT, 5 mM MgCl$_2$, 10% glycerol (vol/vol), 2 mM ATP, 0.05% Digitonin (v/v)), with a phosphate inhibitor (PhosphoStop, Roche Diagnostics). The suspensions were kept on ice for 20 min and then centrifuged twice. Protein concentration was determined with Bio-Rad Protein Assay Kit II and 15 μg sample protein was loaded in a NuPAGE 3–8% Tris-Acetate gel (Thermo Fisher). The gel was run at a constant voltage of 150 V for 4 h. Afterwards, the gel was incubated in an activity buffer (50 mM Tris, 1 mM MgCl$_2$, 1 mM DTT) with 0.05 mM chymotrypsin-like substrate Suc-Leu-Leu-Val-Tyr-AMC (Bachem) for 30 min at 37 °C. The fluorescent signal was measured using ChemiDoc MP (Bio-Rad). The gel was then incubated in a solubilization buffer (2% SDS (w/v), 66 mM Na$_2$CO$_3$, 1.5% 2-Mercaptoethanol (v/v)) for 15 min to prepare the samples for blotting. Through tank transfer, the samples were transferred to a PVDF membrane by 40 mA, overnight and developed as described above. The uncropped images are in Fig. S1.

2.9. Extracellular flux analysis (Seahorse)

Mitochondrial respiration was measured with Seahorse Cell Mito Stress Test (Agilent) with some adjustments to the manufacturer's protocol. Briefly, WT-1 cells were cultured in a 24-well Seahorse plate until day 3 of differentiation. Culture medium was then replaced for Seahorse medium (XF DMEM pH 7.4, 10 mM glucose, 1 mM Pyruvate, 2 mM ʟ-glutamine) and the cells were incubated for 60 min at 37 °C without CO$_2$ before being placed in the Seahorse Analyzer XFe24. In the assay, the cells were treated with NE (final concentration in the well was 1 μM), oligomycin (1 μM), FCCP (4 μM) and μM rotenone–antimycin A (0.5 μM). The reagents were mixed for 3 min, followed by 3 min of incubation, and 3 min of measurements. Afterwards, total DNA was measured for normalization, with CyQUANT Cell Proliferation Assay Kit (Thermo Fisher), according to manufacturer's instructions.

2.10. Statistics

Data were analyzed with ImageLab, Microsoft Excel and Graphpad Prism. Unless otherwise specified, data are shown as mean ± standard error of the mean (SEM), including individual measurements. Multiple student's t-test was used for experiments when comparing two groups and one variable, one-way ANOVA with Tukey post-hoc test was used when comparing three or more groups, and two-ANOVA with Tukey post-hoc test was used for comparing two groups with two variables. P-values lower than 0.05 were considered significant. If groups are significantly different from each other, this is indicated in graphs either with an asterisk (*) or with different letters (a,b). If the same letter is used or nothing is indicated, the groups are statistically indifferent from each other.

3. RESULTS

3.1. *Psmb4* is induced during adipocyte differentiation and regulated by cold

Proteasome function is an evolutionary conserved feature of every mammalian cell, but little is known about the relative presence of
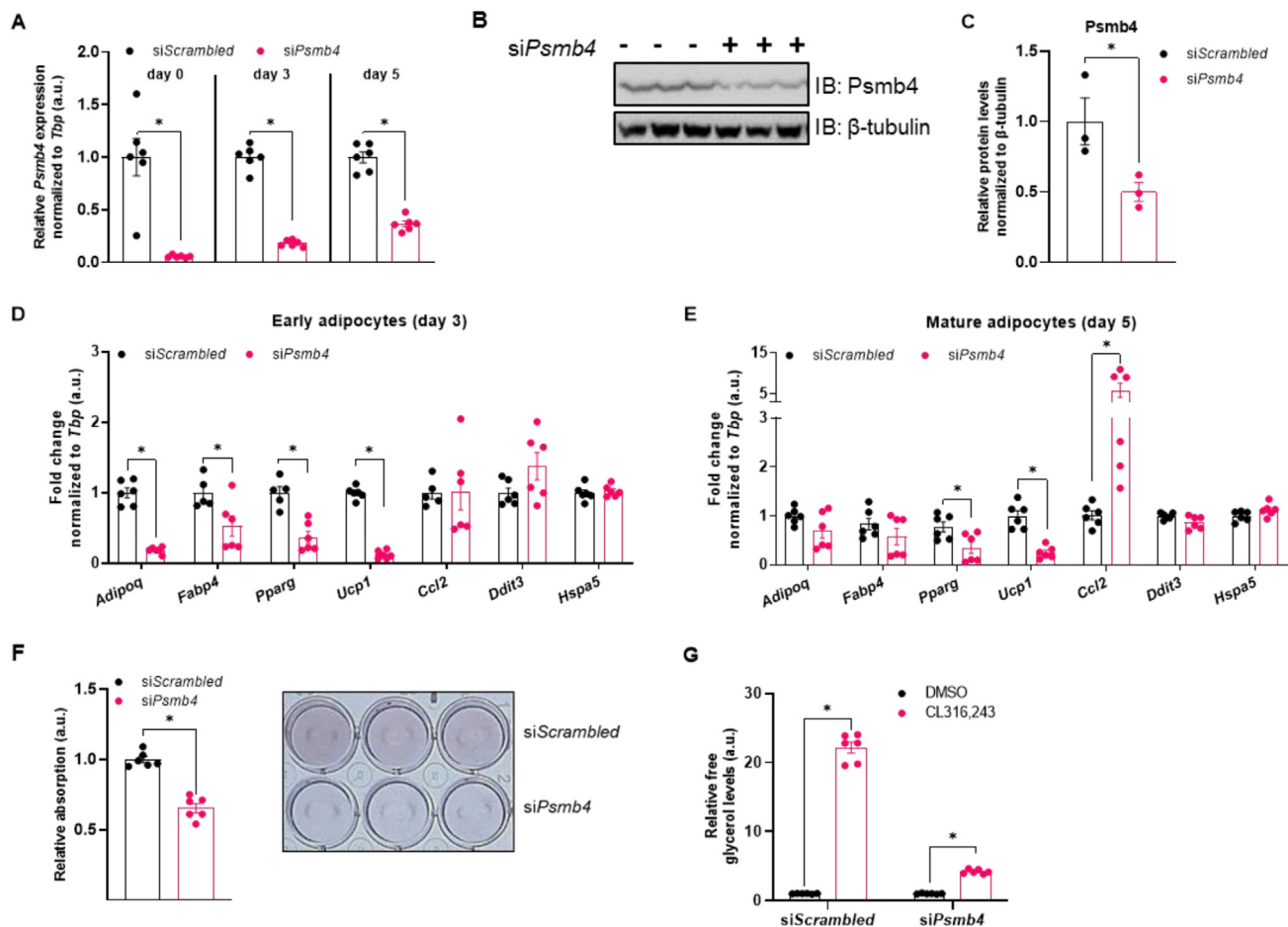
Figure 1: Psmb4 controls adipogenesis and adipocyte health. (A) Relative gene expression of *Psmb4* at different time points after knockdown with scrambled or *Psmb4* siRNA. **(B,C)** Representative immunoblot of Psmb4 in siScrambled and siPsmb4 adipocytes with **(C)** protein quantification normalized to β-tubulin. **(D)** Relative gene expression of adipogenesis and stress markers adipocytes after *Psmb4* knockdown measured on day 3 of differentiation. **(E)** Relative gene expression of adipogenesis and stress markers adipocytes after *Psmb4* knockdown measured on day 5 of differentiation. **(F)** Representative Oil-Red-O staining and quantification (day 5). **(G)** Relative free glycerol levels in adipocyte supernatant (day 5) after DMSO or 1 μM CL316,243 treatment for 3 h. Data are mean ± SEM. Unless otherwise specified: n = 6 independent measurements from 2 separate experiments. Significant if $P < 0.05$, indicated by (*) or different letters.

proteasome subtypes and subunits throughout the body. The PRAAS-linked subunits Psmb4 and Psmb8 are widely and robustly expressed in mouse tissues (Fig. S2A). To better understand expression dynamics in BAT physiology, we compared mice housed at 30 °C (thermoneutrality) and at 4 °C (cold). We found that both genes are robustly expressed in BAT of mice housed at 30 °C thermoneutrality (Fig. S2B). In response to cold, *Psmb4* was unchanged and *Psmb8* expression was lower at 4 °C compared to 30 °C (Fig. S2B). Next, we analyzed cultured brown adipocytes differentiated from immortalized pre-adipocytes. *Psmb4* mRNA levels were markedly higher in differentiated adipocytes compared to pre-adipocytes (Fig. S2C). In contrast, *Psmb8* expression was lower in differentiated adipocytes compared to pre-adipocytes (Fig. S2C). We also tested the response of these genes to pharmacological activation. In line with the in vivo data, *Psmb4* remained unchanged and *Psmb8* was lower in cells activated with NE or the β3-adrenergic agonist CL316,243 (Fig. S2D). In summary, these data show that both *Psmb4* and *Psmb8* are robustly expressed in adipocytes, but while *Psmb4* seems to be implicated in mature brown adipocyte function, *Psmb8* expression was diminished under these conditions. However, to rule out that Psmb8 might nevertheless have

an important function we performed loss-of-function experiments. First, we collected adipose tissues from mice with whole-body deletion of Psmb8 [19] and analyzed gene expression and histology. Mice deficient in Psmb8 had no apparent BAT abnormalities, which also was reflected in unchanged gene expression (Fig. S3A). The notion that Psmb8 is dispensable was supported by in vitro experiments, as silencing of *Psmb8* neither in immortalized pre-adipocytes nor in mature adipocytes produced an impact on adipogenesis or stress markers (Figs. S3B—D). In addition, there was no difference in lipid content in mature adipocytes (Fig. S3E). In conclusion, loss of Psmb8 did not affect adipogenesis or BAT phenotype in vitro or in vivo. The concomitant down-regulation of Psmb8 in response to β3-adrenergic stimulation may indicate that immunoproteasome function is dispensable in brown adipocytes.

3.2. Loss of Psmb4 disrupts adipogenesis and proteostasis
As *Psmb4* was induced during adipocyte differentiation and highly expressed in activated brown adipocytes and BAT, we next studied the role of Psmb4 in brown adipocyte adipogenesis and thermogenic function in more detail. We also investigated if loss of Psmb4 was

associated with cellular stress, assessed by measuring surrogate markers of ER stress and inflammation. Loss of Psmb4 was achieved by silencing *Psmb4* expression through siRNA ("siPsmb4 cells"). Transfection one day before the start of differentiation successfully reduced mRNA levels and this effect remained stable during different stages of adipogenesis (Figure 1A), resulting in lower protein levels (Figure 1B,C). Silencing of Psmb4 led to lower levels of adipogenesis (*Adipoq, Fabp4, Pparg)* and thermogenesis markers (*Ucp1*) during the early phase of adipocyte differentiation (Figure 1D). In mature adipocytes, these changes were less pronounced albeit detectable for *Pparg* and *Ucp1* (Figure 1E). Instead, *Ccl2*, a surrogate marker for the adipocyte stress response [21], was markedly higher in siPsmb4 compared to control cells (Figure 1E). However, ER stress markers *Ddit3* and *Hspa5* did not change upon Psmb4 knockdown (Figure 1D,E). These alterations on transcription level translated to lower lipid content (Figure 1F) and lower lipolysis after treatment with CL316,243 (Figure 1G). PRAAS patients suffer from lipodystrophy in white adipose tissue. Therefore, to complement our findings in WT-1 cells, we also studied the effects of loss of Psmb4 in white adipocytes. For this we used 3T3-L1 cells, immortalized mouse white adipocytes, and knocked down *Psmb4.* Knock-down successfully lowered gene expression (Fig. S4A). si*Psmb4* cells had lower expression of adipogenesis marker *Adipoq* but not *Fabp4*, higher expression of stress markers *Ccl2* and *Cxcl1*, and lower expression of ER stress marker *Ddit3* (Fig. S4B). Silencing *Psmb4* lowered Psmb4 protein levels (Fig. S4C and S4D). In addition, *siPsmb4* cells had lower lipid droplet content and lower baseline lipolysis (Fig. S4E and S4F). Overall, 3T3-L1 cells replicate the effects of loss of Psmb4 on adipogenesis. Altogether, loss of Psmb4 limited adipogenesis and adipocyte function in both brown and white adipocytes.

As Psmb4 is part of the constitutive proteasome, we hypothesized that loss of Psmb4 would disturb UPS and proteostasis. To determine proteasome function in these cells we performed native PAGE analysis, which allows examining activity and protein levels of macromolecular proteasome configurations, i.e., 30S, 26S, and 20S. Chymotrypsin-like peptide hydrolysis activity was lower in siPsmb4 compared to control cells (Figure 2A). On protein level, there were less 20S and 26S complexes present in siPsmb4 cells, as well as an increase in various subcomplexes, including precursors of the 20S proteasome (Figure 2A,B). However, the overall levels of proteasome subunits were unchanged (Figure 2C,D), indicating an assembly deficit of the proteasome in the absence of Psmb4. This is further underscored by higher ubiquitin levels in siPsmb4 compared to control cells (Figure 2E,F). Notably, these changes in UPS were accompanied by higher levels of active Nfe2l1 in the siPsmb4 compared to control cells (Figure 2G,H), indicating that the brown adipocyte mounts an adaptive response to overcome UPS dysfunction. Interestingly, in cell lysates of siPsmb4 compared to control cells, proteasomal activity was lower in immature adipocytes but higher in mature adipocytes (Figure 2I). Complementing the results in WT-1 cells, 3T3-L1 si*Psmb4* cells had higher Nfe2l1 and global ubiquitin levels (Fig. S4C and S4D). In summary, loss of Psmb4 led to proteotoxic stress through proteasome dysfunction as well as limited adipogenesis and adipocyte function.

3.3. Activation of Nfe2l1 partially compensates for the loss of Psmb4
While loss of Psmb4 had a marked effect on proteasome function, it did not completely disable UPS. We hypothesized that the activation of Nfe2l1 mitigated some of the effects of Psmb4 silencing. Therefore, we tested whether the adipocyte phenotype was more severe in a double

Psmb4 and *Nfe2l1* knockdown model. Double knockdown successfully led to lower mRNA as well as protein levels of both Psmb4 and Nfe2l1 (Figure 3A−E). Double knockdown also inhibited the Nfe2l1-mediated increase in proteasome subunits on protein and gene expression level (Figure 3B−D). Indeed, double knockdown of both *Nfe2l1* and *Psmb4* led to lower proteasomal activity compared to control cells or single gene silencing (Figure 3E). The effects of the double knockdown of *Psmb4* and *Nfe2l1* on adipogenesis markers compared to control or the single knockdown cells were minimal (Figure 3F). However, *Psmb4* knockdown was associated with higher adipocyte inflammation surrogate markers compared to control cells, but this effect was not further amplified by additional *Nfe2l1* knockdown (Figure 3G). In addition, loss of Psmb4 led to markedly higher mRNA levels of *Activating Transcription Factor-3 (Atf3)*, an important transcription factor linked to the integrated stress response, but not of other stress markers (Figure 3H), which is also seen in PRAAS patients [5]. These changes were independent of *Nfe2l1* knockdown (Figure 3H). In summary, activation of Nfe2l1 helps to sustain proteasome function upon loss of Psmb4, but this effect did neither restore adipogenesis nor reduce the adipocyte stress response under these conditions.

3.4. Atf3 links loss of Psmb4 to inflammation and adipogenesis
The fact that Atf3 expression was selectively induced in siPsmb4 cells caught our attention, as Atf3 is a stress-induced transcription factor that reportedly has been associated with adipogenesis and lipogenesis [22]. To investigate the role of Atf3 in our model system, we silenced *Psmb4*, *Nfe2l1* or *Atf3* individually and in a paired fashion (Figure 4A). This approach did not affect the viability of the adipocytes (Figure 4B). Unlike targeting Nfe2l1, *Atf3* knockdown in addition to *Psmb4* knockdown did not affect proteasomal activity (Figure 4C). However, *Atf3* knockdown in addition to *Psmb4* knockdown normalized the expression of the inflammation markers *Ccl2 and Cxcl1* compared to siPsmb4 and control cells (Figure 4D). In line with this normalized gene expression pattern, double knockdown of both *Psmb4* and *Atf3* largely rescued lipogenesis and restored lipolysis as follows. Particularly, cells with double knockdown of *Psmb4* and *Atf3* displayed markedly higher lipid content compared to si*Psmb4* cells, and similar lipid content compared to control cells (Figure 4E). Knockdown of only *Atf3* or *Nfe2l1* had no effect. Brown adipocytes with double knockdown of *Psmb4* and *Atf3* displayed higher NE-induced glycerol release compared to si*Psmb4* cells, cancelling out the effect of si*Psmb4* (Figure 4F). Again, knockdown of only *Atf3* or *Nfe2l1* had no effect. (Figure 4F). To verify whether the effects on lipolysis were caused by changes in lipogenesis or lipolysis, we measured expression of essential lipases involved in degradation of triglycerides. Expression levels of Adipose triglyceride lipase (Atgl, encoded by *Pnpla2*), Hormone sensitive lipase (Hsl, endoced by *Lipe),* and Monoglyceride lipase (Mgll, encoded by *Mgll*) were not affected by si*Psmb4* (Figure 4G). Therefore, the effect of *Psmb4* knockdown on glycerol release was due to a lower triglyceride content, and not altered lipolysis activity. Finally, to assess NST, we measured NE-stimulated oxygen consumption followed by a mitochondrial stress test using a Seahorse Analyzer. In line with the finding that loss of Psmb4 diminishes brown adipocyte function, si*Psmb4* cells displayed abolished NE-stimulated and uncoupled respiration as well as lower maximal capacity compared to control cells. Double knockdown of both *Psmb4* and *Atf3* largely rescued these alterations in mitochondrial function (Figure 4H,I). Knockdown of only *Atf3* or *Nfe2l1* had no effect (Figure 4H,I). In conclusion, loss of Psmb4 disrupts adipogenesis and thermogenesis through the activation of Atf3.
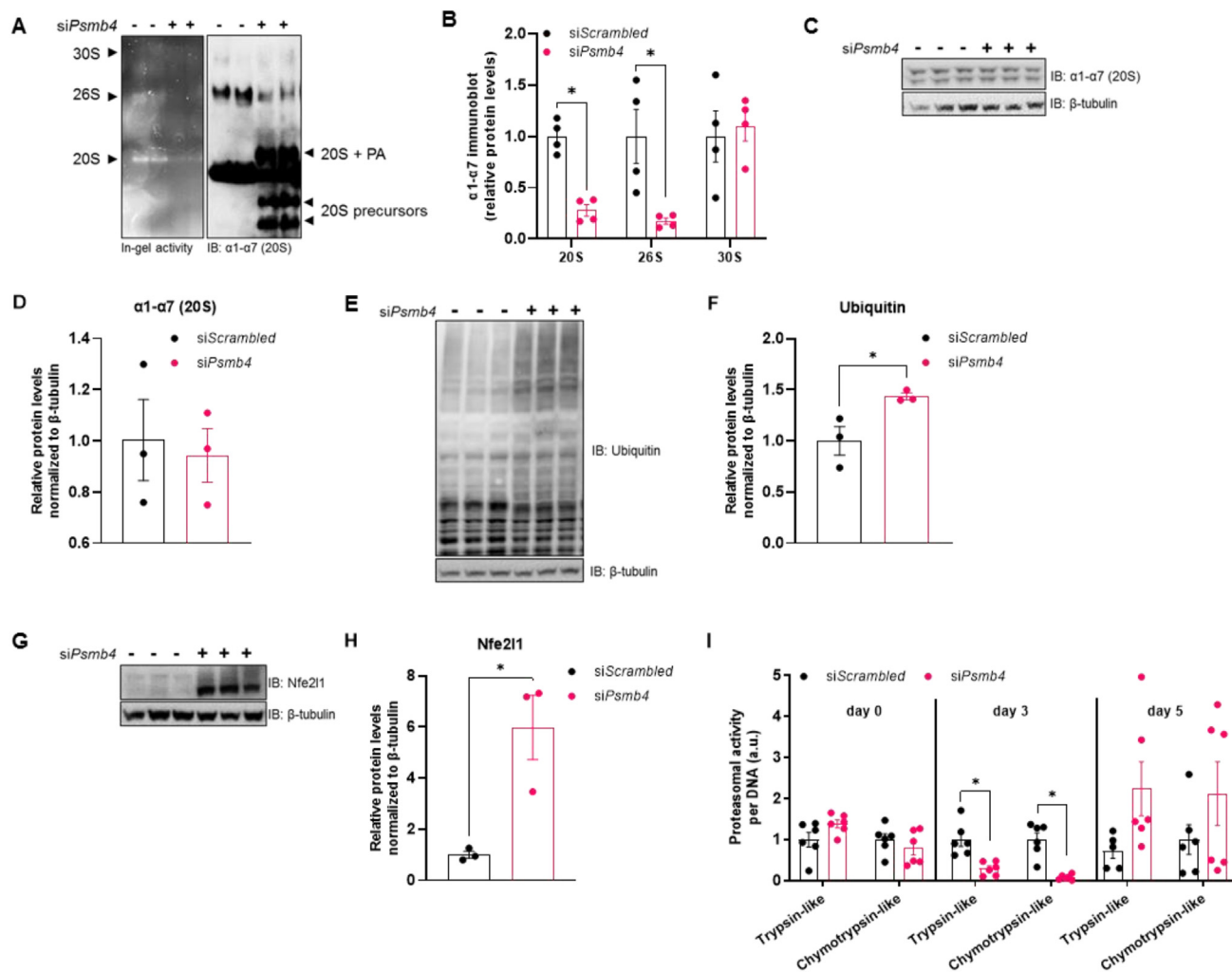
Figure 2: Psmb4 controls UPS and proteostasis. (A) Representative Native PAGE with in-gel chymotrypsin-like proteasome activity and immunoblot of $\alpha1$-$\alpha7$ (20S) proteasome subunits. (PA: proteasome activators) **(B)** Relative protein levels $\alpha1$-$\alpha7$ (20S) proteasome subunits measured in Native PAGE immunoblots. **(C,D)** Representative immunoblot of $\alpha1$-$\alpha7$ (20S) proteasome subunits from adipocytes (day 5) with **(D)** protein quantification relative to β-tubulin. **(E,F)** Representative immunoblot of ubiquitin from adipocytes (day 5) with **(F)** protein quantification relative to β-tubulin. **(G,H)** Representative immunoblot of Nfe2l1 from adipocytes (day 5) with **(D)** protein quantification relative to β-tubulin. **(I)** Trypsin-like and chymotrypsin-like proteasome activity in adipocytes at different time points, normalized to DNA content. Data are mean $\pm$ SEM. Unless otherwise specified: n = 6 independent measurements from 2 separate experiments. Significant if $P < 0.05$, indicated by (*) or different letters.

4. DISCUSSION

The proteasome is considered a prerequisite for cellular proteostasis, but its remodeling in response to processes of physiologic adaptation remains largely unexplored. PRAAS syndrome has shed light on the relevance of the proteasome in human pathology, but the underlying molecular mechanisms linking disturbed proteasome function to e.g., inflammation and lipodystrophy remains unclear. Here, we show that in mouse brown and white adipocytes loss of Psmb4 disturbs proteostasis and protein quality control and, thus, impacts adipogenesis and thermogenesis. In contrast, *Psmb8* silencing had no effect. In these cells, *Psmb4* is a constitutively expressed gene that is upregulated during adipogenesis and states of thermogenic activation. *Psmb4* is a target gene of Nfe2l1 and this regulation is in line with the general requirement of increased proteasome function during cold adaptation [15]. Contrasting this, *Psmb8* encodes for a subunit of the immunoproteasome subunit, which is induced by interferons. Psmb8 ablation was previously shown to disrupt proteostasis in immune response

[5,19]. As the role of the immunoproteasome is especially important in hematopoietic cells [23,24], it is perhaps logical that Psmb8 expression diminishes during differentiation, as there is little requirement for a mature adipocyte. Considering this, it is not surprising that Psmb8 is dispensable for brown adipocyte development and function.

PRAAS patients with mutations in *PSMB4* or *PSMB8* have a similar disease presentation [5] and suffer from lipodystrophy and fevers. Our data suggest that the intrinsic cellular pathways may vary in these patients. It is possible that lipodystrophy in patients with *PSMB8* mutations is a result of autoinflammation and its systemic effects on adipose tissue whereas lipodystrophy in patients with *PSMB4* mutations is caused by a combination of the autoinflammatory syndrome and intrinsically impaired adipogenesis. Our results do not suggest that hyperactivation of BAT is involved in the fever symptoms in patients, as loss of Psmb4 function in mouse brown adipocytes diminishes NST. Nevertheless, altered thermoregulation in the absence of NST might contribute to the symptoms. In addition, we are aware that silencing of genes by RNAi does not completely reflect the natural effects of
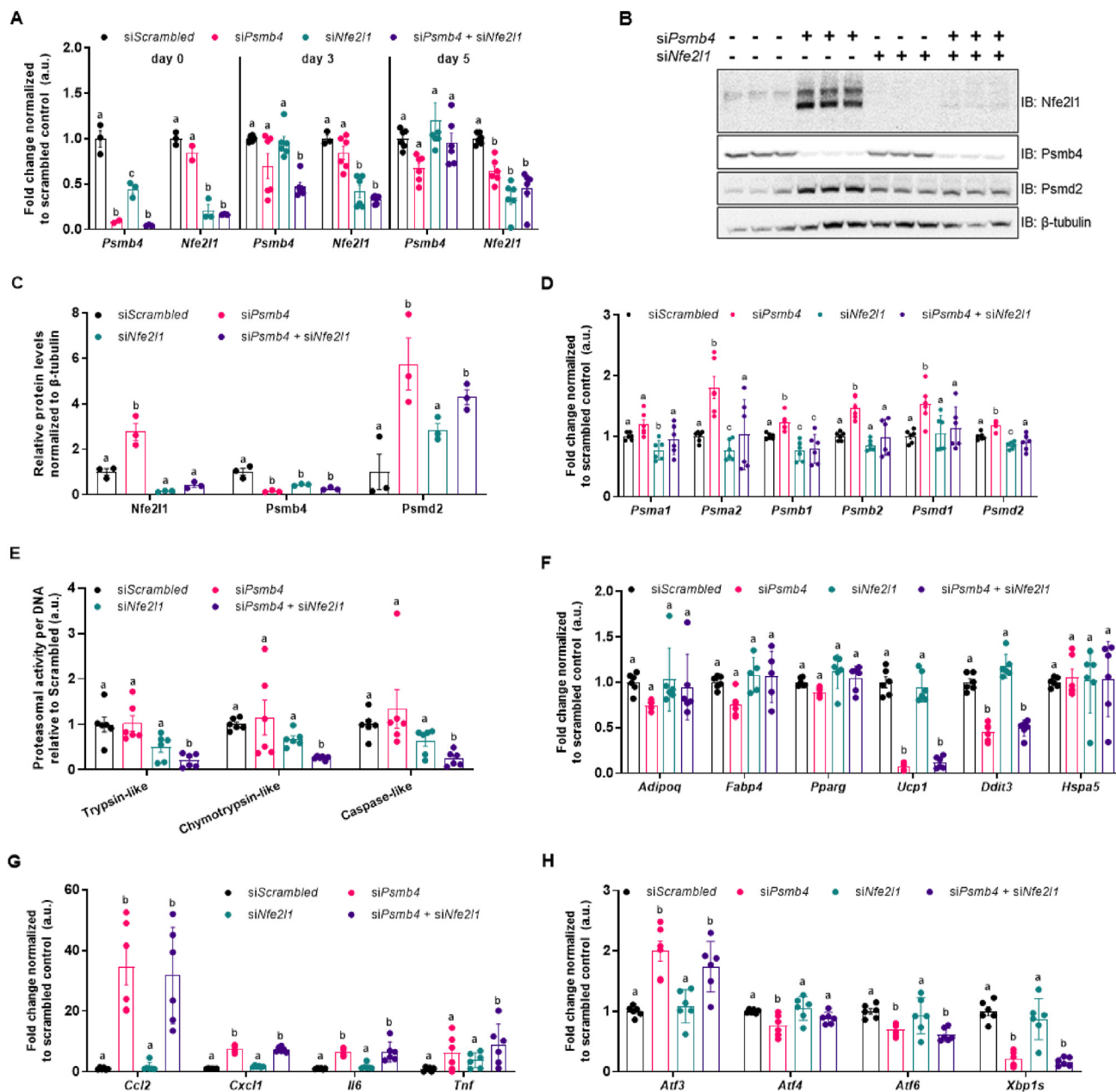
Figure 3: Loss of Psmb4 initiates a proteostatic stress-response via Nfe2l1. (A) Relative gene expression of *Psmb4* and *Nfe2l1* at different time points after knockdown with scrambled, *Psmb4* and/or *Nfe2l1* siRNA. **(B,C)** Representative immunoblots of Nfe2l1, Psmb4, Psmd2 and β-tubulin in siScrambled, siPsmb4, siNfe2l1 or siPsmb4 + siNfe2l1 adipocytes (day 5) with **(C)** protein quantification levels normalized to β-tubulin. **(D)** Relative gene expression of various proteasome subunits. **(E)** Trypsin-like, chymotrypsin-like, and caspase-like proteasome activity in adipocytes (day 5), normalized to DNA content. **(F)** Relative gene expression of adipogenesis and stress markers in adipocytes (day 5). **(G)** Relative gene expression of inflammation markers in adipocytes (day 5). **(H)** Relative gene expression of ER stress and unfolded protein response markers in adipocytes (day 5). Data are mean ± SEM. Unless otherwise specified: n = 6 independent measurements from 2 separate experiments. Significant if $P < 0.05$, indicated by (*) or different letters.

missense, truncation, or deletion mutations in patients. However, our study warrants further investigation of *PSMB4* mutations on proteasome and adipocyte function. A more complete understanding of systemic as well as cell-specific effects, could improve treatment options for patients.

An interesting and potentially therapeutically relevant aspect of our work is the adaptive activation of Nfe2l1 in response to loss of Psmb4 in adipocytes. This recruitment of Nfe2l1 is most likely a response to insufficient turnover of ubiquitinated proteins caused by proteasome dysfunction, as seen in PRAAS patients [25] or by inhibiting

proteasome activity with chemical inhibitors [12]. While the activation of Nfe2l1 partly restored total proteasomal activity, we found that this activation of Nfe2l1 was insufficient to overcome the defects in adipogenesis and adipocyte function. Perhaps, while both the loss of Psmb4 and Nfe2l1 cause abnormal proteasomal function, a major difference between the two conditions is the presence of incomplete proteasome intermediates. Reduced total proteasomal activity in the absence of Nfe2l1 was not associated with incomplete proteasome intermediates, and, consequently, also not with a block in adipogenesis. More work is needed to characterize the complex remodeling
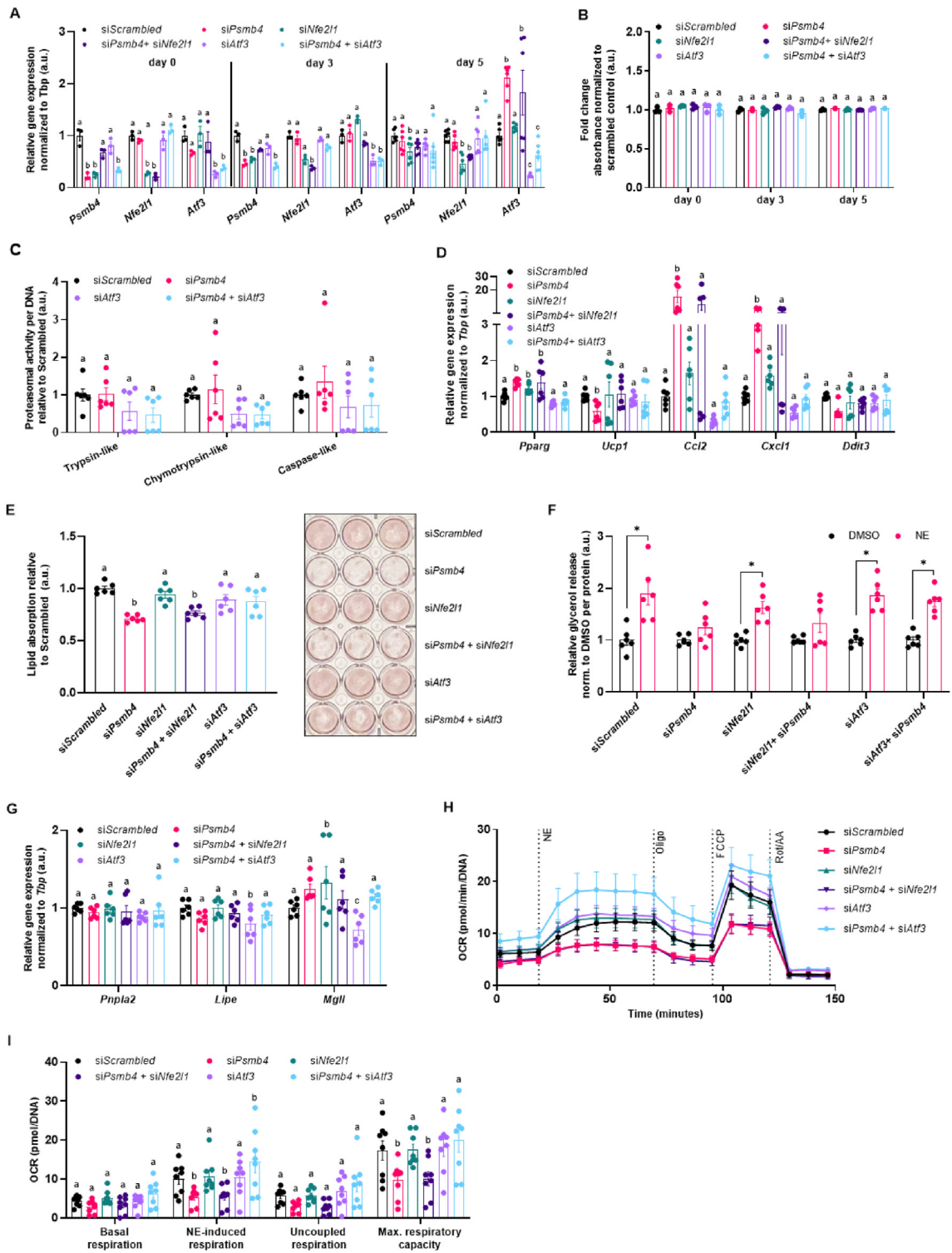
Figure 4: Loss of Psmb4 induces inflammation and blocks adipogenesis via Atf3. (A) Relative gene expression of *Psmb4*, *Nfe2l1*, and *Atf3*. **(B)** Viability in adipocytes. **(C)** Trypsin-like, chymotrypsin-like, and caspase-like proteasome activity in adipocytes (day 5), normalized to DNA content **(D)** Relative gene expression of adipogenesis and stress markers in adipocytes (day 5) after knockdown. **(E)** Oil-Red-O staining in adipocytes after knockdown. **(F)** Supernatant free glycerol levels after treatment with DMSO or 1 μM Norepinephrine (NE) for 1 h normalized to protein. **(G)** Relative gene expression of lipases in adipocytes (day 5). **(H, I)** Oxygen consumption rate (OCR) in adipocytes after knockdown, normalized to DNA levels (n = 8, from 2 experiments). Unless otherwise specified: n = 6 independent measurements from 2 separate experiments. Data are mean ± SEM. Significant if $P < 0.05$, indicated by (*) or different letters.

of cellular proteasome function under proteotoxic stress conditions. Nfe2l1 activation might serve as a therapeutic approach to overcome some of the pathologies associated with PRAAS.

A major finding of our study is that silencing of *Atf3* largely rescued the adipocyte defects caused by loss of Psmb4. Atf3 is a member of the mammalian activation transcription factor/cAMP responsive element-binding (CREB) protein family of transcription factors that responds to various stressors [22] and is a downstream target of Atf4 [26]. Interestingly, Atf3 was previously shown to downregulate adipogenesis markers and to protect against diet-induced obesity in mice [27]. In the context of our research, Atf3 could be viewed as a brake that responds to proteotoxic stress caused by loss of Psmb4. Atf3 does not seem to signal back to the UPS or predispose the cell death, yet its activation induces inflammatory pathways, potentially sending out "danger" and "help" signals. Removing Atf3 clears the path for adipogenesis, lipid metabolism and thermogenesis and might be of therapeutic interest to tackling symptoms associated with PRAAS.

More generally, in the broader context of metabolism, our data underscore the relevance of UPS-mediated protein quality control in maintaining cellular health and function, exemplified here in the context of adipocytes. We show that proteostasis and lipid metabolism are intricately linked in adipocytes and failure to secure proteostasis results in diminished adipogenesis. An important hallmark of obesity-induced adipocyte dysfunction is cellular stress and inflammation, which are tightly linked to aberrant lipid metabolism and insulin resistance. Our finding that maladaptation of UPS and the activation of stress sensors, including Atf3, impede adipogenesis should also be interpreted in the context of potentially hampering obesity-induced adipose tissue expansion or, as in the case of PRAAS, resulting in lipodystrophy. Identifying the key nodes linking proteostasis to cellular stress pathways will represent an important step towards understanding pathological alterations that result in aberrant metabolism, inflammation, premature ageing, and cancer.

AUTHOR CONTRIBUTIONS

N.W. and I.A. performed the experiments and analyzed data. M.S.T. and E.K. provided the mouse model and mouse samples. N.W. and A.B. conceptually designed the study, interpreted the data, and wrote the manuscript. All authors read and commented on the manuscript.

FUNDING

ACKNOWLEDGMENTS

CONFLICT OF INTEREST

None declared.

APPENDIX A. SUPPLEMENTARY DATA

Supplementary data to this article can be found online at https://doi.org/10.1016/j.molmet.2022.101518.

REFERENCES

[1] Torrelo, A., Patel, S., Colmenero, I., Gurbindo, D., Lendínez, F., Hernández, A., et al., 2010 Mar. Chronic atypical neutrophilic dermatosis with lipodystrophy and elevated temperature (CANDLE) syndrome. Journal of the American Academy of Dermatology 62(3):489—495.

[2] Agarwal, A.K., Xing, C., DeMartino, G.N., Mizrachi, D., Hernandez, M.D., Sousa, A.B., et al., 2010 Dec. PSMB8 encoding the β5i proteasome subunit is mutated in Joint Contractures, muscle atrophy, microcytic anemia, and panniculitis-induced lipodystrophy syndrome. The American Journal of Human Genetics 87(6):866—872.

[3] Kanazawa, N., 2012. Nakajo-nishimura syndrome: an autoinflammatory disorder showing pernio-like rashes and progressive partial lipodystrophy. Allergology International 61(2):197—206.

[4] Kitamura, A., Maekawa, Y., Uehara, H., Izumi, K., Kawachi, I., Nishizawa, M., et al., 2011 Oct 3. A mutation in the immunoproteasome subunit PSMB8 causes autoinflammation and lipodystrophy in humans. Journal of Clinical Investigation 121(10):4150—4160.

[5] Brehm, A., Liu, Y., Sheikh, A., Marrero, B., Omoyinmi, E., Zhou, Q., et al., 2015 Oct 20. Additive loss-of-function proteasome subunit mutations in CANDLE/PRAAS patients promote type I IFN production. Journal of Clinical Investigation 125(11):4196—4211.

[6] Ebstein, F., Poli Harlowe, M.C., Studencka-Turski, M., Krüger, E., 2019 Nov 26. Contribution of the unfolded protein response (UPR) to the pathogenesis of proteasome-associated autoinflammatory syndromes (PRAAS). Frontiers in Immunology 10:2756.

[7] Finley, D., 2009 Jun. Recognition and processing of ubiquitin-protein conjugates by the proteasome. Annual Review of Biochemistry 78(1):477—513.

[8] Collins, G.A., Goldberg, A.L., 2017 May. The logic of the 26S proteasome. Cell 169(5):792—806.

[9] Kimura, H., Caturegli, P., Takahashi, M., Suzuki, K., 2015. New insights into the function of the immunoproteasome in immune and nonimmune cells. J Immunol Res 2015:1—8.

[10] Huber, E.M., Basler, M., Schwab, R., Heinemeyer, W., Kirk, C.J., Groettrup, M., et al., 2012 Feb. Immuno- and constitutive proteasome crystal structures reveal differences in substrate and inhibitor specificity. Cell 148(4):727—738.

[11] Mann, J.P., Savage, D.B., 2019 Aug 5. What lipodystrophies teach us about the metabolic syndrome. Journal of Clinical Investigation 129(10):4009—4021.

[12] Cannon, B., Nedergaard, J., 2004 Jan. Brown adipose tissue: function and physiological significance. Physiological Reviews 84(1):277—359.

[13] Bartelt, A., Bruns, O.T., Reimer, R., Hohenberg, H., Ittrich, H., Peldschus, K., et al., 2011 Feb. Brown adipose tissue activity controls triglyceride clearance. Natura Med 17(2):200—205.

[14] Lemmer, I.L., Willemsen, N., Hilal, N., Bartelt, A., 2021 Jan. A guide to understanding endoplasmic reticulum stress in metabolic disorders. Molecular Metabolism 47:101169.

[15] Bartelt, A., Widenmaier, S.B., Schlein, C., Johann, K., Goncalves, R.L.S., Eguchi, K., et al., 2018 Mar. Brown adipose tissue thermogenic adaptation requires Nrf1-mediated proteasomal activity. Natura Med 24(3):292—303.

[16] Radhakrishnan, S.K., Lee, C.S., Young, P., Beskow, A., Chan, J.Y., Deshaies, R.J., 2010 Apr. Transcription factor Nrf1 mediates the proteasome recovery pathway after proteasome inhibition in mammalian cells. Molecular Cell 38(1):17—28.

[17] Sha, Z., Goldberg, A.L., 2014 Jul. Proteasome-mediated processing of Nrf1 is essential for coordinate induction of all proteasome subunits and p97. Current Biology 24(14):1573—1583.

[18] Fehling, H.J., Swat, W., Laplace, C., Kühn, R., Rajewsky, K., Müller, U., et al., 1994 Aug 26. MHC class I expression in mice lacking the proteasome subunit LMP-7. Science 265(5176):1234—1237.

[19] Seifert, U., Bialy, L.P., Ebstein, F., Bech-Otschir, D., Voigt, A., Schröter, F., et al., 2010 Aug. Immunoproteasomes preserve protein homeostasis upon interferon-induced oxidative stress. Cell 142(4):613—624.

[20] Yazgili, A.S., Meul, T., Welk, V., Semren, N., Kammerl, I.E., Meiners, S., 2021 Jun. In-gel proteasome assay to determine the activity, amount, and composition of proteasome complexes from mammalian cells or tissues. STAR Protoc 2(2):100526.

[21] Rull, A., Camps, J., Alonso-Villaverde, C., Joven, J., 2010. Insulin resistance, inflammation, and obesity: role of monocyte chemoattractant protein-1 (orCCL2) in the regulation of metabolism. Mediators of Inflammation 2010:1—11.

[22] Ku, H.-C., Cheng, C.-F., 2020 Aug 14. Master regulator activating transcription factor 3 (ATF3) in metabolic homeostasis and cancer. Frontiers in Endocrinology 11:556.

[23] Çetin, G., Klafack, S., Studencka-Turski, M., Krüger, E., Ebstein, F., 2021 Jan 5. The ubiquitin—proteasome system in immune cells. Biomolecules 11(1):60.

[24] Tubío-Santamaría, N., Ebstein, F., Heidel, F.H., Krüger, E., 2021 Jun 22. Immunoproteasome function in normal and malignant hematopoiesis. Cells 10(7):1577.

[25] Sotzny, F., Schormann, E., Kühlewindt, I., Koch, A., Brehm, A., Goldbach-Mansky, R., et al., 2016 Dec. TCF11/Nrf1-Mediated induction of proteasome expression prevents cytotoxicity by rotenone. Antioxid Redox Signal 25(16):870—885.

[26] Forsström, S., Jackson, C.B., Carroll, C.J., Kuronen, M., Pirinen, E., Pradhan, S., et al., 2019 Dec. Fibroblast growth factor 21 drives dynamics of local and systemic stress responses in mitochondrial myopathy with mtDNA deletions. Cell Metabolism 30(6):1040—1054 e7.

[27] Ku, H.-C., Chan, T.-Y., Chung, J.-F., Kao, Y.-H., Cheng, C.-F., 2022 Jan. The ATF3 inducer protects against diet-induced obesity via suppressing adipocyte adipogenesis and promoting lipolysis and browning. Biomed Pharmacother Biomedecine Pharmacother 145:112440.